Supporting Information

Instantaneous Degradation of Nerve Agent Simulants using Zirconium-based Metal-organic Polyhedra

Kimia Kiaei,[a] Andrzej Gładysiak,[a] Kieran Brunson,[a] Kyle Smith,[a] Kye Hunter,[b] Ava Thomas,[a] Delaney Radke,[a] Tim Zuehlsdorff, [b] and Kyriakos C. Stylianou[a]*

[a]*Materials Discovery Laboratory (MaD Lab), Department of Chemistry, Oregon State University, Corvallis, OR, 97331-4003 USA*

[b]*Department of Chemistry, Oregon State University, Corvallis, OR, 97331-4003, USA*

Experimental Procedures

S1. Materials and methods

S1.1. Materials

Zirconocene dichloride, 2-aminoterephthalic acid, terephthalic acid, trimesic acid, and *N,N*-diethylformamide (DEF) were purchased from TCI America.

S1.2. Synthesis of Zr-BDC-NH_2 [1]

Zirconocene dichloride (17.5 mg, 0.06 mmol) was mixed with 2-aminoterephthalic acid (5.4 mg, 0.03 mmol) in a 1 dram vial. DEF was added to the mixture (0.5 mL) followed by 150 µL of DI H_2O. The mixture was sonicated until all solid particles were dissolved, resulting in a clear yellow solution. The vial was then left in a preheated oven at 60 °C for 8 hours, followed by cooling to room temperature for 4 hours. Cube-shaped yellow crystals were obtained. The crystals were filtered and collected for characterization. PXRD, FT-IR, BET, and solid state UV-Vis measurements were performed on the obtained crystals. The molecular formula of the Zr-BDC-NH_2 cage is: $\{[Cp_3Zr_3O(OH)_3]_4(BDC\text{-}NH_2)_6\}\cdot$anions·guest molecules; Cp^-: cyclopentadienyl, BDC^{2-}: benzene 1,4-dicarboxylate.

S1.3. Synthesis of Zr-BDC [2]

Zirconocene dichloride (17.5 mg, 0.06 mmol) was mixed with terephthalic acid (5.0 mg, 0.03 mmol) in a 1 dram vial. DEF was added to the mixture (0.5 mL) followed by 150 µL of DI H_2O. The mixture was sonicated until all solid particles were dissolved, resulting in a clear colorless solution. The vial was then left in a preheated oven at 60 °C for 8 hours, followed by cooling to room temperature for 4 hours. Cube-shaped crystals were obtained. The crystals were filtered and collected for characterization. PXRD, FT-IR, BET, and solid state UV-Vis measurements were performed on the obtained crystals. The molecular formula of the Zr-BDC cage is: $\{[Cp_3Zr_3O(OH)_3]_4(BDC)_6\}\cdot$anions·guest molecules.

S1.4. Synthesis of Zr-BTC [2]

Zirconocene dichloride (17.5 mg, 0.06 mmol) was mixed with trimesic acid (8.4 mg, 0.04 mmol) in a 1 dram vial. DEF was added to the mixture (0.5 mL) followed by 150 µL of DI H_2O. The mixture was sonicated until all solid particles were dissolved, resulting in a clear colorless solution. The vial was then left in a preheated oven at 60 °C for 8 hours, followed by cooling to room temperature for 4 hours. Elongated crystals were obtained. The crystals were filtered and collected for characterization. PXRD, FT-IR, BET, and solid state UV-Vis measurements were performed on the obtained crystals. The molecular formula of the Zr-BTC

cage is: $\{[Cp_3Zr_3O(OH)_3]_4(BTC)_4\}\cdot$anions$\cdot$guest molecules; BTC^{3-}: benzene-1,3,5-tricarboxylate.

S1.5. Characterization Techniques

Powder X-ray diffraction was performed using a Rigaku MiniFlex600 benchtop diffractometer. Powdered samples were packed onto silicon wafer zero-background sample holders and their diffraction patterns were measured in the 3–30° 2θ region in Bragg–Brentano geometry with monochromatized Cu Kα radiation and a 1D detector.

The DMNP hydrolysis was evaluated using a Bruker 500 MHz NMR spectrometer.

Fourier-transform infrared (FT-IR) spectra were obtained using a PerkinElmer Spectrum Two FT-IR spectrometer.

Nitrogen isotherms at 77 K were collected on as-synthesized samples on a Micromeritics 3Flex surface area characterization analyzer.

Scanning electron microscopy (SEM) on MOP samples was performed using an FEI QUANTA 600FEG environmental SEM. Samples were coated with Au-Pd using a vacuum evaporator before collecting the SEM micrographs.

Elemental analysis was performed using a UNICUBE (Elementar) CHNSO microelemental analyzer.

Mass spectrometry measurements was conducted with a Waters SYNAPT G2 Time of Flight mass spectrometer in resolution mode. Two different ion sources were used; 1) Atmospheric Pressure Gas Chromatography (APGC) in positive ion mode. APGC was used in "Rapid Shotgun" mode, a one meter section of deactivated silica tubing is used instead of a GC column. Instrument settings: Helium carrier gas, corona needle, voltage 2.4 kV, cone voltage 30 V, source temperature 140 °C. 1 µL injection volume. 2) Electrospray Ionization (ESI) mode, both positive and negative ion modes were analyzed. Loop injections of 1µL were analyzed (no column). Source temperature 100 °C, spray voltage 3.0 kV, cone voltage 30 V. A Waters I Class UPLC was used for sample introduction. Water: Acetonitrile:0.1% formic acid (50:50%) was used as carrier solvent. The flow rate was 0.1 mL/min. MassLynx software was used to process the data.

Solvent exchange was performed by liquid–liquid exchange with *n*-hexane. A 1 dram vial was used instead of a separatory funnel. The reaction solution (0.4 mL) was mixed with 0.4 mL *n*-hexane solvent. The mixture was vigorously stirred and left to form separated layers for 30 minutes. The *n*-hexane phase was then removed from the top with a pipette and was taken for GC-MS analysis.

The same experiments were repeated for the *n*-hexane solvent using a GC column.

Thermogravimetric analysis (TGA) was performed using a SDT Q600 TA Instruments apparatus on a temperature range of room temperature to 600 °C.

S1.6. DMNP hydrolysis experiments

MOP powder (0.0006 mmol (per Zr-sites)), was added to a 1 dram vial. A 0.45M solution of *N*-ethylmorpholine (NEM) buffer in D_2O was prepared and 0.4 mL of the buffer solution was added to the 1 dram vial. The MOP-buffer solution was then stirred using a Vortex mixer for the MOP to completely disperse in the solution. The DMNP source for this study was a 0.08 M solution of DMNP in methanol and 12.5 μL of this solution (0.001 mmol of DMNP) was added to the vial. The amount of each component in the reaction solution consisted of 0.18 mmol NEM, 22.169 mmol of D_2O, and 0.3 mmol methanol from the DMNP solution. The vial was then stirred using a Vortex mixer for certain reaction time periods (from 30 seconds to 5 minutes), and was diluted by adding 0.4 mL more of the NEM solution. Then the solution of filtered and transferred to an NMR tube with a syringe for characterization.

Control experiment was performed the same way as mentioned above, with no catalyst.

To calculate the half-life of catalyst reaction, following the pseudo-first order kinetic model a linear fitting of the natural log of DMNP concentration vs. time of reaction was performed.

S1.7. Computational methods

To calculate the binding energies of cyclopentadiene and DMNP for MOP Zr-BCD, the MOP was truncated to a single zirconium cluster with three dicarboxyphenyl groups and appropriate zirconium bound ligands. Optimized geometries and their relative energies were calculated using the Gaussian [3] software package, and used the CAM-B3LYP [4] DFT functional with a mixed basis of 6-31+G* [5–11] on nonmetals and a Stuttgart-Dresden effective core potential [12] for zirconium. The surrounding environment was treated as a polarizable medium [13] with the dielectric constant of methanol, and Grimme's semi-empirical dispersion correction.[14] Binding energies were calculated from the difference of total energy of the bound complex and the sum of energies of the two unbonded groups. Several possible coordinations of DMNP to MOP were optimized and compared.

Table S1. Elemental analysis of the MOPs.

Material	Formula	Elements	Theory	Found
Zr-BDC	$\{[Cp_3Zr_3O(OH)_3]_4(BDC)_6\}Cl_4 \cdot 12DMF \cdot 8H_2O$	C	40.30	40.31
		H	4.60	4.65
		N	3.92	4.14
Zr-BDC-NH_2	$\{[Cp_3Zr_3O(OH)_3]_4(BDC\text{-}NH_2)_6\}Cl_4 \cdot 18DMF \cdot 5H_2O$	C	39.47	39.10
		H	4.65	4.88
		N	5.75	5.47
Zr-BTC	$\{[Cp_3Zr_3O(OH)_3]_4(BTC)_4\}Cl_4 \cdot 6DMF \cdot 4H_2O$	C	37.12	38.16
		H	3.66	3.41
		N	2.28	3.17
Zr-BTC after catalysis	$\{[Cp_3Zr_3O(OH)_3]_4(BTC)_4\}Cl_4 \cdot 1DMF \cdot 18H_2O \cdot 1CH_3OH$	C	33.90	34.02
		H	3.73	3.48
		N	0.40	0.35

Figures

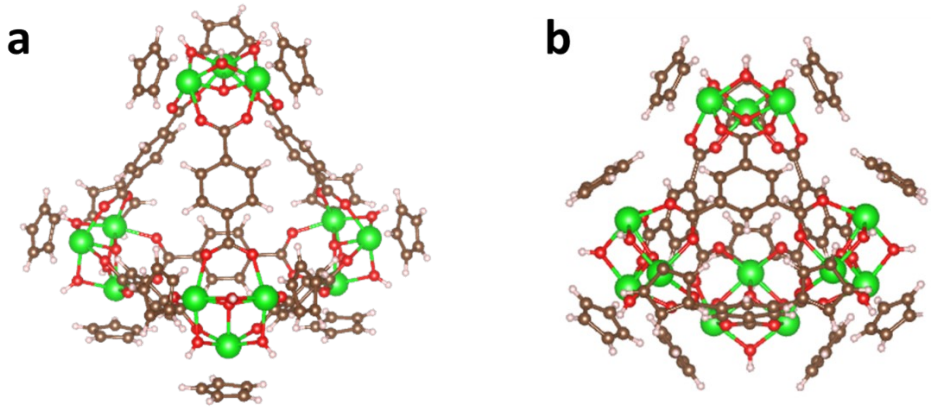

Figure S1. The structures of **a. Zr-BDC** and **b. Zr-BTC** MOPs demonstrating tetrahedral cage shape. BDC and BTC ligands are on the edges and faces of the tetrahedron, respectively. The Zr clusters are located on the corners with a Cp^- capping ligand for each Zr atom (figure made using VESTA software[15]).

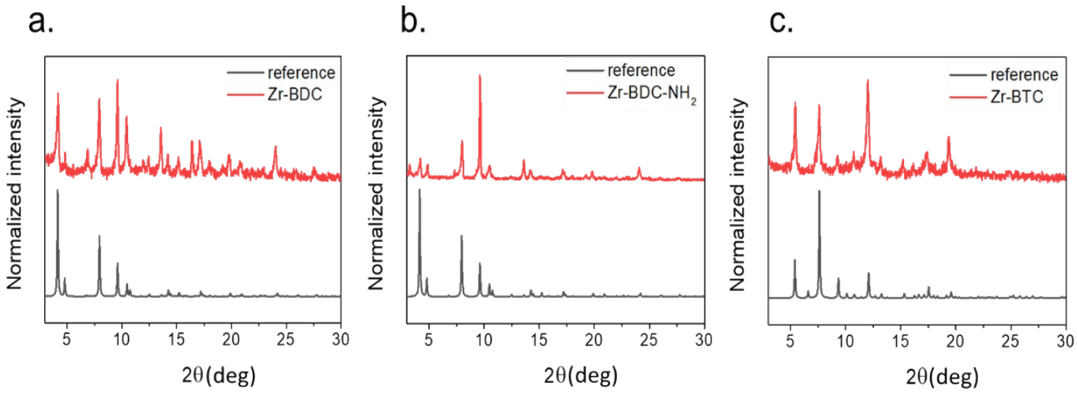

Figure S2. PXRD patterns for the as-synthesized MOPs: a. **Zr-BDC**, b. **Zr-BDC-NH_2**, c. **Zr-BTC**. The simulated patterns for all three MOPs are taken from the crystallographic data provided in the report by Liu et al.[2]

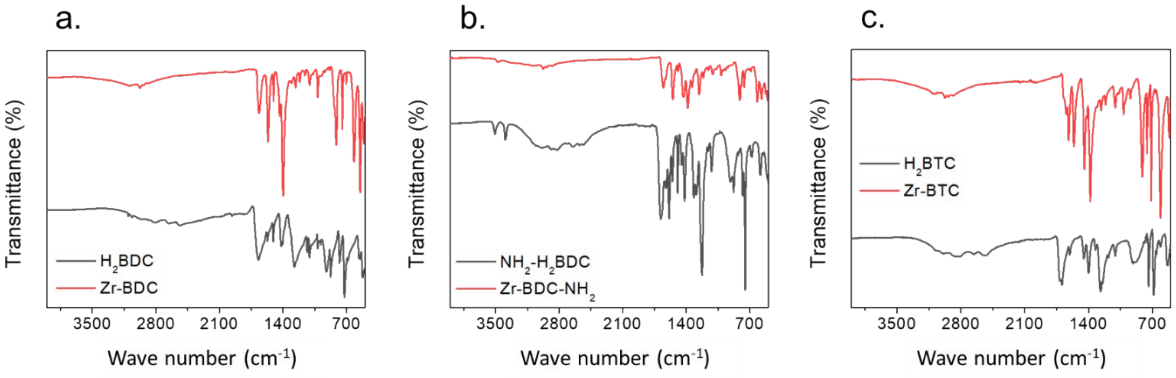

Figure S3. the FT-IR spectra of MOPs and their corresponding precursor ligands: a. **Zr-BDC**, b. **Zr-BDC-NH$_2$**, c. **Zr-BTC**.

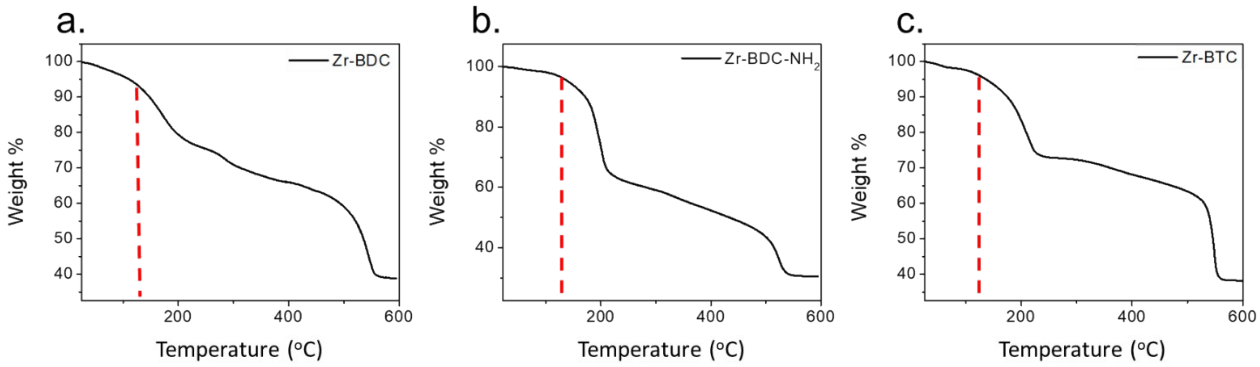

Figure S4. TGA curves of as-synthesized MOPs: a. **Zr-BDC**, b. **Zr-BDC-NH$_2$**, c. **Zr-BTC**.

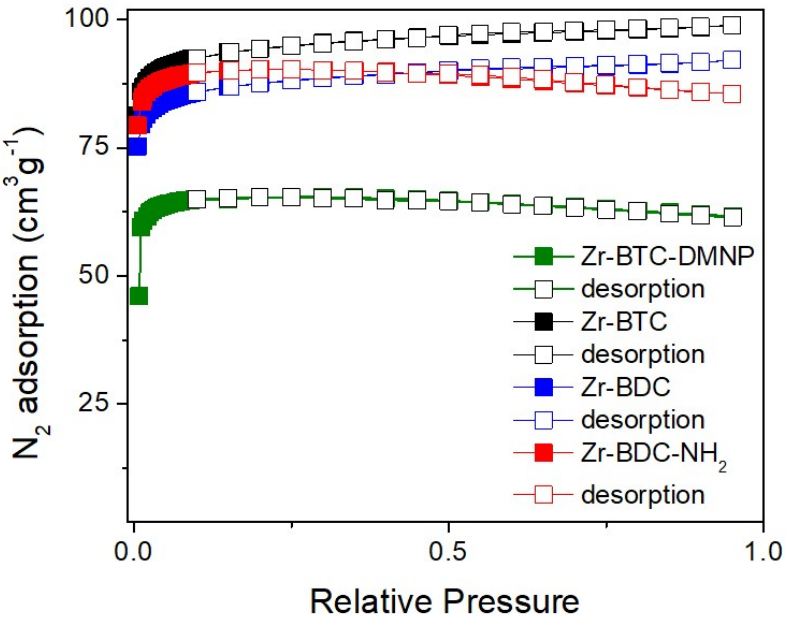

Figure S5. N_2 adsorption-desorption isotherms. All MOPs were gently activated at 60 °C for 24 h before gas sorption analysis.The calculated BET surface area for the as-synthesized **Zr-BTC**, **Zr-BDC** and **Zr-BDC-NH$_2$** is 365 m^2g^{-1}, 338 m^2g^{-1}, and 298 m^2g^{-1}, respectively. The BET surface area of **Zr-BTC** after DMNP degradation (Zr-BTC-DMNP) is reduced to 265 m^2g^{-1}.

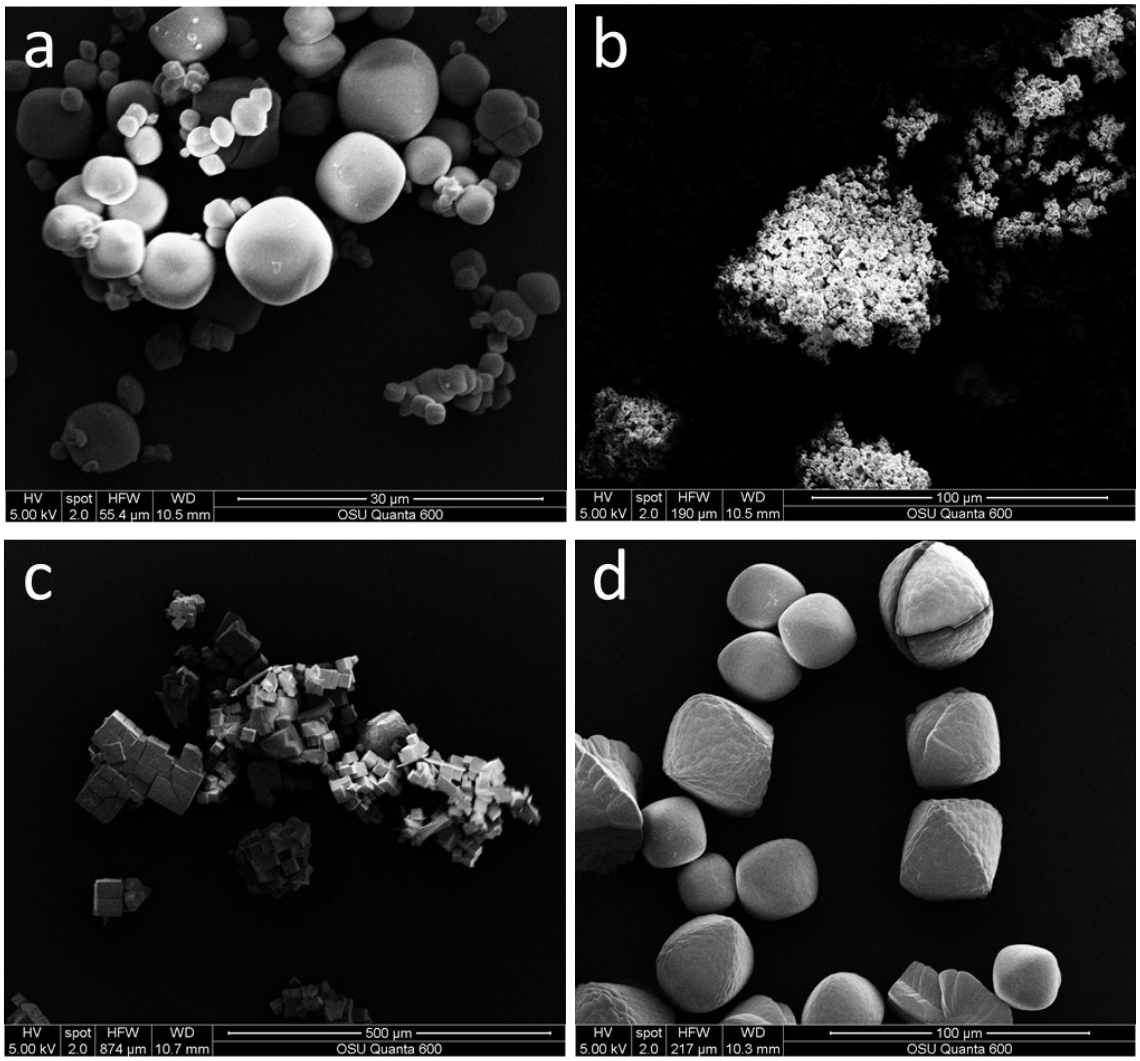

Figure S6. SEM micrographs of as-synthesized (a) **Zr-BTC**, (b) **Zr-BDC**, and (c) **Zr-BDC-NH_2**. (d) shows the SEM micrograph of **Zr-BTC** after DMNP degradation.

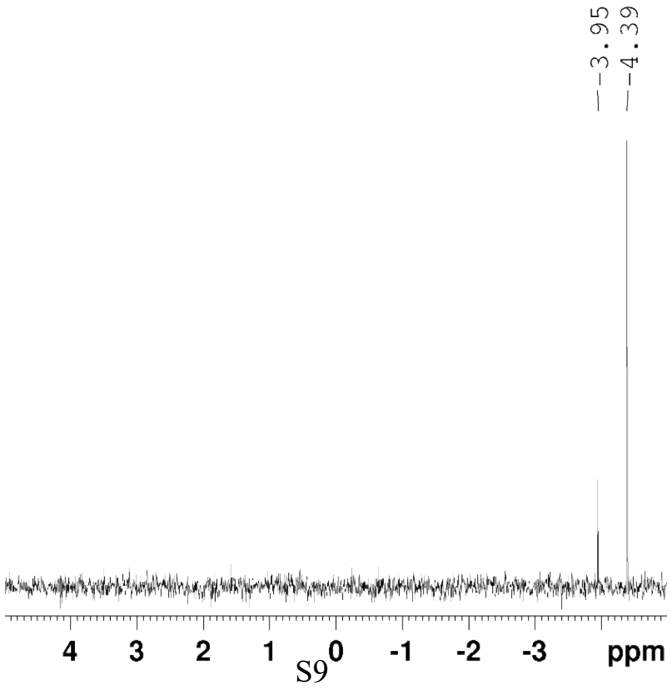

Figure S7. ^{31}P-NMR spectra of the background degradation of DMNP in buffered solution after 5 minutes. The -4.39 ppm peak belongs to DMNP and the -3.95 ppm peak belongs to M4NP, a byproduct of degradation.

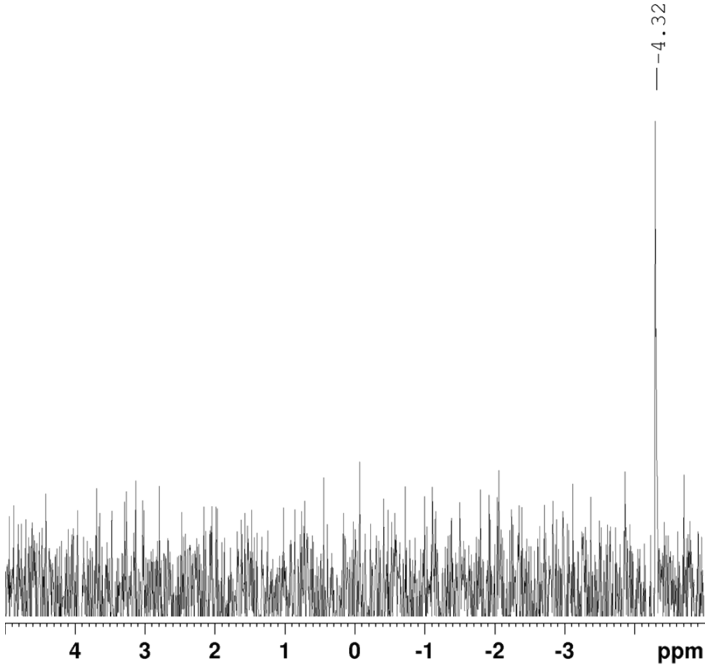

Figure S8. ^{31}P-NMR spectra of DMNP degradation in buffered solution after 5 minutes with zirconocene dichloride in buffered solution.

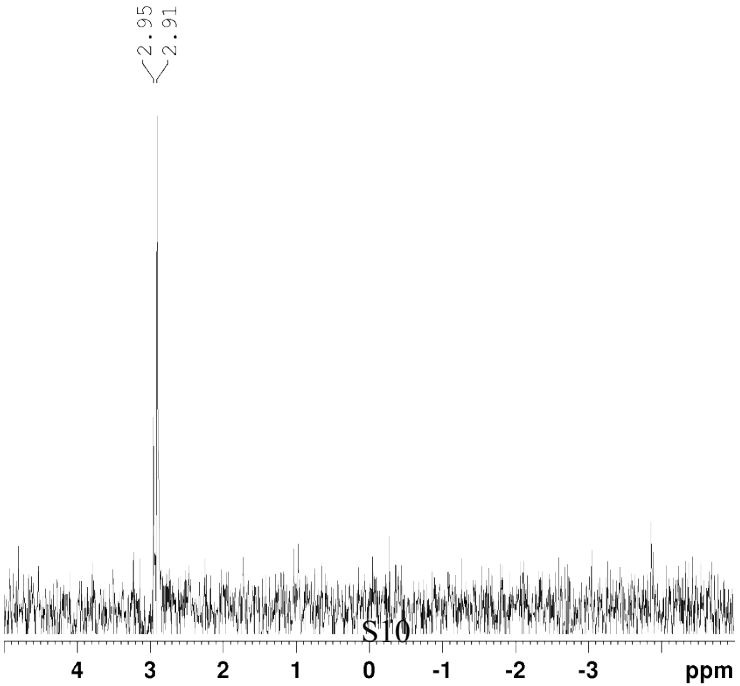

Figure S9. ^{31}P-NMR spectra of second cycle of degradation of DMNP with **Zr-BTC** catalyst in buffered solution after 3 min.

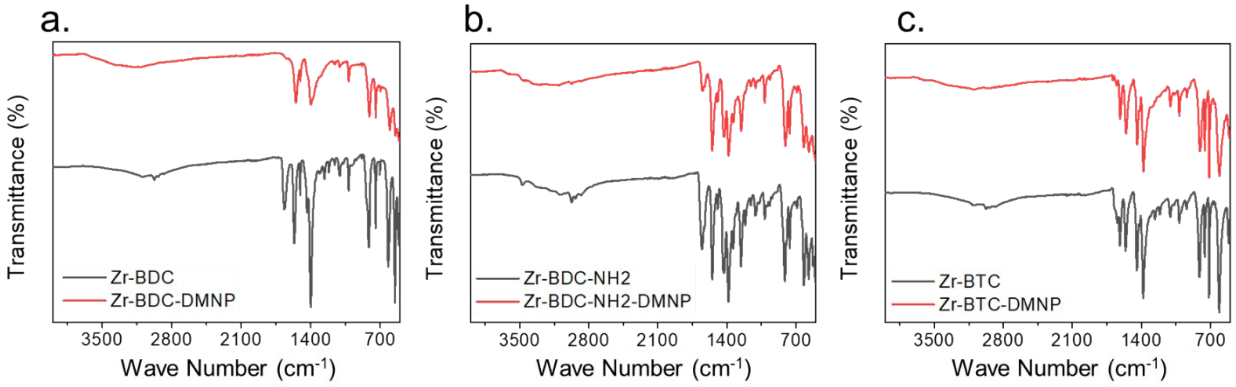

Figure S10. FT-IR spectra of the MOPs before and after DMNP degradation: a. **Zr-BDC**, b. **Zr-BDC-NH$_2$**, c. **Zr-BTC**.

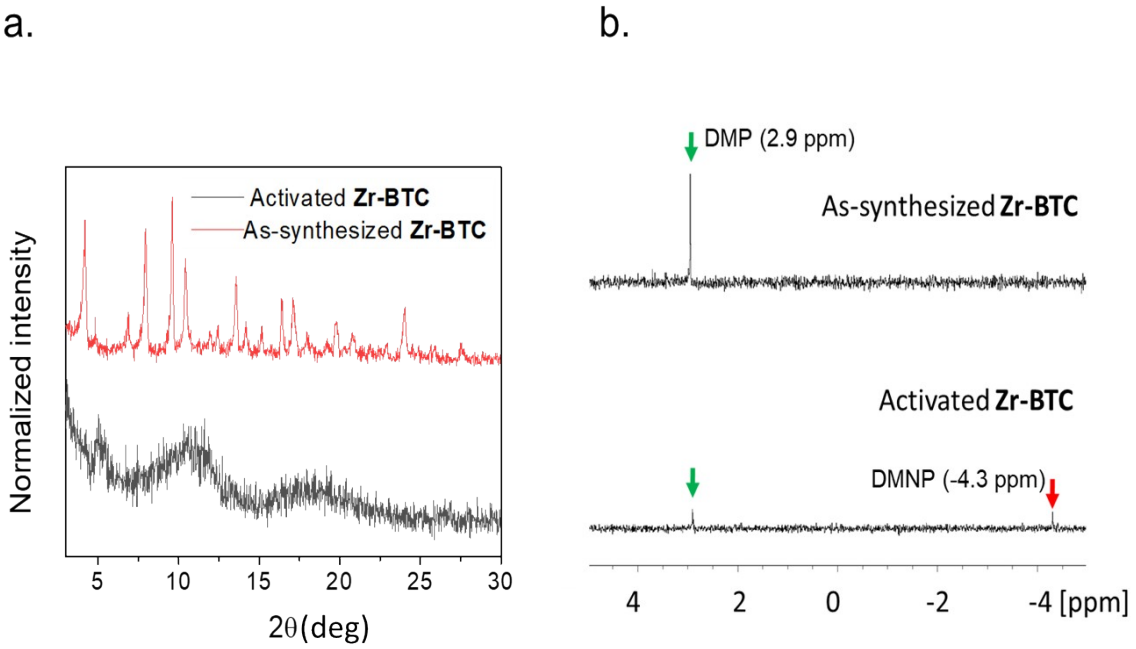

Figure S11. a. PXRD patterns of the activated and as-synthesized Zr-BTC. **b.** ^{31}P-NMR spectra showing DMNP degradation after 2 minutes for the activated and as-synthesized **Zr-BTC**. DMP is the degradation product of DMNP.

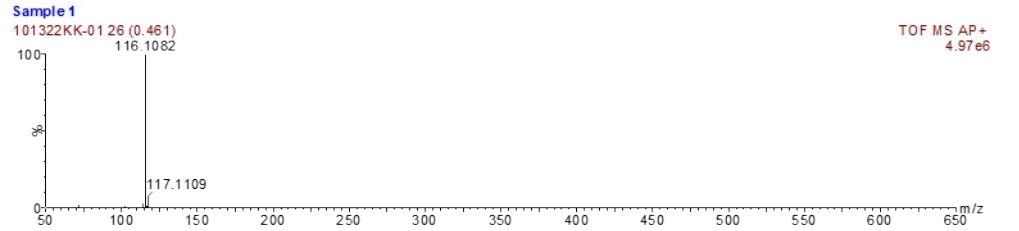
Sample 1
101322KK-01 26 (0.461)
TOF MS AP+
4.97e6
116.1082
117.1109
m/z

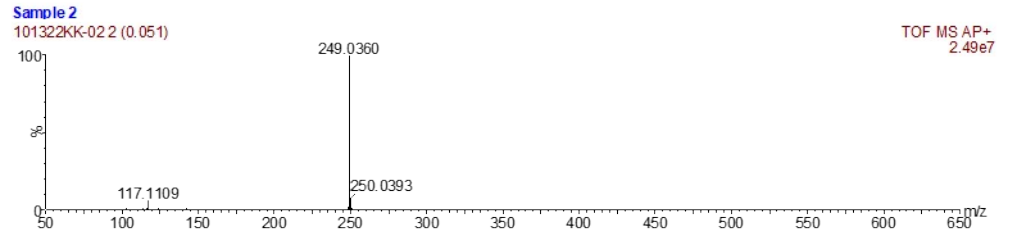
Sample 2
101322KK-02 2 (0.051)
TOF MS AP+
2.49e7
249.0360
250.0393
117.1109
m/z

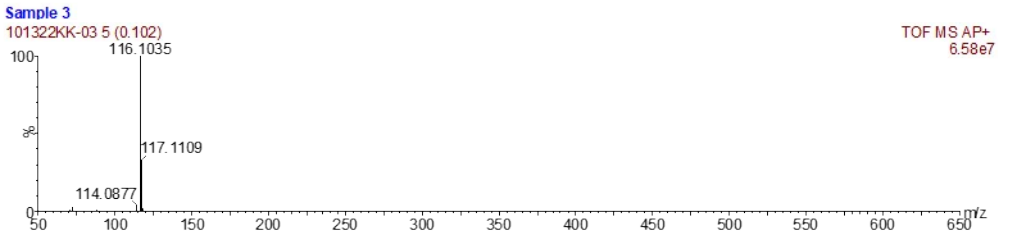
Sample 3
101322KK-03 5 (0.102)
TOF MS AP+
6.58e7
116.1035
117.1109
114.0877
m/z

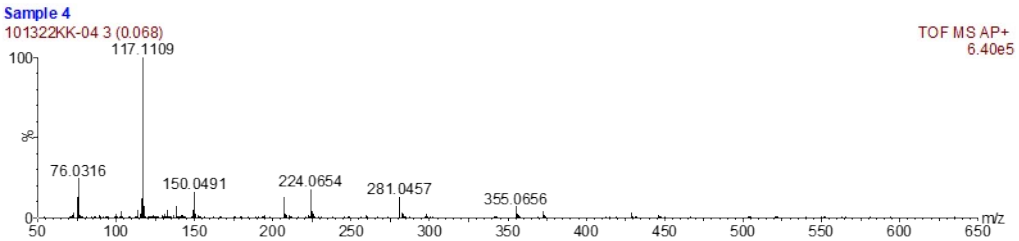
Sample 4
101322KK-04 3 (0.068)
TOF MS AP+
6.40e5
117.1109
76.0316
150.0491
224.0654
281.0457
355.0656
m/z

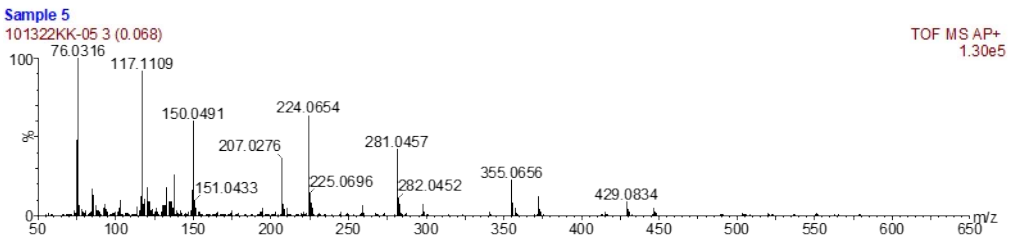
Sample 5
101322KK-05 3 (0.068)
TOF MS AP+
1.30e5
76.0316
117.1109
150.0491
224.0654
207.0276
281.0457
151.0433
225.0696
282.0452
355.0656
429.0834
m/z

Figure S12. APGC-Mass-spectra for the **Zr-BTC** reaction solution (Sample 1), DMNP (Sample 2), N-ethylmorpholine buffer solution (Sample 3), Trimesic acid ligand (Sample 4), and Zirconocene dichloride (Sample 5).

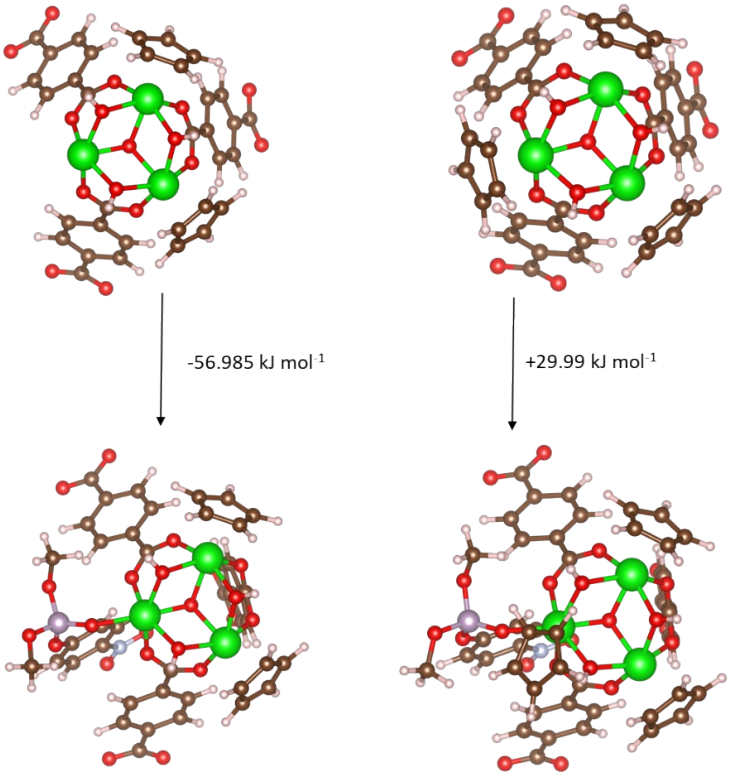

Figure S13. Demonstration of bond energies for the attachment of DMNP and Cp^- groups in **Zr-BDC**.

References

1 D. Nam, J. Huh, J. Lee, J. H. Kwak, H. Y. Jeong, K. Choi and W. Choe, *Chem. Sci.*, 2017, **8**, 7765–7771.

2 G. Liu, Z. Ju, D. Yuan and M. Hong, *Inorg. Chem.*, 2013, **52**, 13815–13817.

3 M. J. Frisch, G. W. Trucks, H. B. Schlegel, G. E. Scuseria, M. a. Robb, J. R. Cheeseman, G. Scalmani, V. Barone, G. a. Petersson, H. Nakatsuji, X. Li, M. Caricato, a. V. Marenich, J. Bloino, B. G. Janesko, R. Gomperts, B. Mennucci, H. P. Hratchian, J. V. Ortiz, a. F. Izmaylov, J. L. Sonnenberg, Williams, F. Ding, F. Lipparini, F. Egidi, J. Goings, B. Peng, A. Petrone, T. Henderson, D. Ranasinghe, V. G. Zakrzewski, J. Gao, N. Rega, G. Zheng, W. Liang, M. Hada, M. Ehara, K. Toyota, R. Fukuda, J. Hasegawa, M. Ishida, T. Nakajima, Y. Honda, O. Kitao, H. Nakai, T. Vreven, K. Throssell, J. a. Montgomery Jr., J. E. Peralta, F. Ogliaro, M. J. Bearpark, J. J. Heyd, E. N. Brothers, K. N. Kudin, V. N. Staroverov, T. a. Keith, R. Kobayashi, J. Normand, K. Raghavachari, a. P. Rendell, J. C. Burant, S. S. Iyengar, J. Tomasi, M. Cossi, J. M. Millam, M. Klene, C. Adamo, R. Cammi, J. W. Ochterski, R. L. Martin, K. Morokuma, O. Farkas, J. B. Foresman and D. J. Fox, 2016, Gaussian 16, Revision C.01, Gaussian, Inc., Wallin.

4 T. Yanai, D. P. Tew and N. C. Handy, *Chem. Phys. Lett.*, 2004, **393**, 51–57.

5 T. Clark, J. Chandrasekhar, G. W. Spitznagel and P. V. R. Schleyer, *J. Comput. Chem.*, 1983, **4**, 294–301.

6 R. Ditchfield, W. J. Hehre and J. A. Pople, *J. Chem. Phys.*, 2003, **54**, 724.

7 M. M. Francl, W. J. Pietro, W. J. Hehre, J. S. Binkley, M. S. Gordon, D. J. DeFrees and J. A. Pople, *J. Chem. Phys.*, 1998, **77**, 3654.

8 M. S. Gordon, J. S. Binkley, J. A. Pople, W. J. Pietro and W. J. Hehre, *J. Am. Chem. Soc.*, 1982, **104**, 2797–2803.

9 P. C. Hariharan and J. A. Pople, *Theor. Chim. acta 1973 283*, 1973, **28**, 213–222.

10 W. Kohn and L. J. Sham, *Phys. Rev.*, , DOI:10.1103/PhysRev.140.A1133.

11 G. W. Spitznagel, T. Clark, P. von Ragué Schleyer and W. J. Hehre, *J. Comput. Chem.*, 1987, **8**, 1109–1116.

12 D. Andrae, U. Häußermann, M. Dolg, H. Stoll and H. Preuß, *Theor. Chim. acta 1990 772*, 1990, **77**, 123–141.

13 J. Tomasi, B. Mennucci and R. Cammi, *Chem. Rev.*, 2005, **105**, 2999–3093.

14 S. Grimme, J. Antony, S. Ehrlich and H. Krieg, *J. Chem. Phys.*, 2010, **132**, 154104.

15 K. Momma and F. Izumi, *J. Appl. Crystallogr.*, 2011, **44**, 1272–1276.